metals

MDPI

Article

Achieving High Self-Lubricating Performance of Al-Bi-Sm-Ti Alloys Based on the Intermetallic Compounds

Tiannan Man [1,2], Lin Zhang [1], Zhisheng Nong [2], Shaowei Lu [2,*] and Engang Wang [1,*]

[1] Key Laboratory of Electromagnetic Processing of Materials (Ministry of Education), Northeastern University, Shenyang 110004, China; manxiaoxiao165@163.com (T.M.); zhanglin@epm.neu.edu.cn (L.Z.)
[2] School of Materials Science and Engineering, Shenyang Aerospace University, Shenyang 110136, China; nzsfir@163.com
* Correspondence: lushaowei_2005@163.com (S.L.); egwang@mail.neu.edu.cn (E.W.); Tel./Fax: +86-248-368-1739 (E.W.)

Abstract: Al-Bi immiscible alloys, as wear resistance material, have attracted increasing attention in the past. The solidification processing of alloys plays a significant role in the final solidification microstructure and properties of immiscible alloys. Here, we present a strategy to produce a homogeneous microstructure in Al-Bi alloys based on intermetallic compounds. With the addition of Sm and Ti, the effect on the microstructure and properties was discussed in detail. The Al-Bi-Sm-Ti alloys achieve high self-lubricating performance, referring to the values of the coefficient of friction and wear rate. The intermetallic compounds formed were regarded as the main anti-friction and anti-wear factors. The results of numerical simulation indicate that microsegregation in Al-Bi alloys was retarded based on the intermetallic compounds. The coefficient of friction of the Al-Bi-1Sm-2Ti alloy was 46.2% lower than that of the Al-Bi alloys at 300 m. This research provides a new perspective and guidance for designing and fabricating composites with superior self-lubricating properties.

Keywords: immiscible alloys; intermetallic compounds; self-lubricating performance

check for updates

Citation: Man, T.; Zhang, L.; Nong, Z.; Lu, S.; Wang, E. Achieving High Self-Lubricating Performance of Al-Bi-Sm-Ti Alloys Based on the Intermetallic Compounds. *Metals* **2023**, *13*, 1836. https://doi.org/10.3390/met13111836

Academic Editors: Emin Bayraktar and Jean-Louis Bobet

Received: 15 August 2023
Revised: 14 October 2023
Accepted: 16 October 2023
Published: 1 November 2023

Correction Statement: This article has been republished with a minor change. The change does not affect the scientific content of the article and further details are available within the backmatter of the website version of this article.

Copyright: © 2023 by the authors. Licensee MDPI, Basel, Switzerland. This article is an open access article distributed under the terms and conditions of the Creative Commons Attribution (CC BY) license (https://creativecommons.org/licenses/by/4.0/).

1. Introduction

Immiscible alloys have a wide range of applications due to their special physical and chemical properties. Immiscible alloys have been investigated due to their special microstructure. The characteristics of immiscible alloys are dependent on both the composition and the microstructure. However, the phase diagrams of immiscible alloys show a wide miscibility gap in the liquid state. It is therefore very difficult to obtain a uniform distribution of the Bi phase owing to the liquid–liquid separation [1–4].

Al-Bi immiscible alloys could replace materials for self-lubricated bearings in the near future. The Al-Bi alloys are much easier and cheaper to mass produce and thus more suitable for applications. However, liquid phase separation deteriorates the mechanical and wear properties of the Al-Bi alloys formed by conventional casting. The microstructure evolution of the Al-Bi immiscible alloy during liquid phase separation is a result of the concurrent actions of nucleation, growth, Ostwald ripening, motion, and collision coagulation of the minority phase droplets [5–7].

Al-Bi alloys have aroused great interest and considerable investigations have been conducted with respect to microstructure evolution and optimal alloy design by using different techniques. However, immiscible alloys inevitably undergo liquid phase separation during the solidification process, usually resulting in individual immiscible phases. Al-Bi immiscible alloys inherit all of the inherent characteristics of the constituent Al and Bi. This property arises from the alloy's microstructure, which is a strength matrix with a well-dispersed soft phase. With the development of high-speed and high-load engines, there is a higher demand for improved strength and wear performance of Al-Bi alloys [8–10]. To effectively meet the requirements, it is urgently necessary to fabricate well-dispersed microstructures

with superior self-lubricating properties. The self-lubricating wear resistance of Al-Bi immiscible alloys arises from the strength of the Al matrix with a well-dispersed soft Bi phase. Therefore, control of the dispersion of Bi-rich droplets can potentially improve the performance of Al-Bi immiscible alloys [11–15].

Recently, Cao et al. reported W nanoparticles incorporated into a Zn-Bi immiscible alloy to prevent Bi sedimentation. Liquid phase separation was controlled by the addition of W nanoparticles [16]. As indicated by these results, adding other elements is an effective way to produce controllably refined and homogeneous microstructures in immiscible alloys [17]. However, ex situ particles reinforced Al-Bi immiscible alloys are susceptible to cracking due to heat damage of the ceramic phases during processing. To overcome such a disadvantage, in situ particles in Al-Bi immiscible alloys have been developed, because they can offer a variety of new properties, such as high strength and high wear resistance, when Bi-rich particles are dispersed in an Al-rich matrix due to liquid phase separation [18–20]. To expand the industrial applications of Al-Bi immiscible alloys, we chose the in situ intermetallic compounds to overcome the microstructure segregation and low wear resistance [21].

In this paper, the Ti and Sm elements were first added into Al-Bi immiscible alloys. The solidification behavior and microstructure of the Al-Bi-Sm-Ti system were influenced due to the intermetallic compounds. By comparing the friction coefficient and wear rates, the effects of the intermetallic compounds on the wear properties of Al-Bi alloys were investigated. Based on the experimental results, the self-lubricating mechanisms of alloys were proposed.

2. Experimental Procedures

The Al-20Bi-Sm-Ti alloys were prepared in a high-frequency induction furnace under an Ar atmosphere. The Al, Ti, and Sm were first melted in an alundum crucible. Then, 20 wt% Bi was added to the melt. The phase diagram of Al-Bi alloys is shown in Figure 1. The Ti and Sm were packaged in two layers of Al foil to protect it from oxidization and feed powder into the melt. To guarantee the homogenization of the samples, the ingot was held for 10 min at 1100 °C and then cooled down in water.

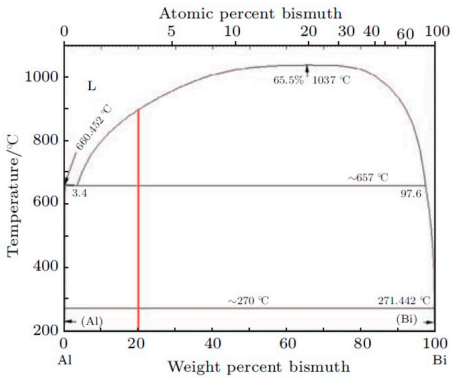


Figure 1. The phase diagram of Al-Bi alloys.

A JSM-6360LV scanning electron microscope (SEM) equipped with energy dispersive spectroscopy was used to characterize the microstructures of the alloys. The phase structures were examined by X-ray diffraction on a D/Max-2500PC X-ray diffractometer using a CuKa line. Hardness tests were carried out on sample polished surfaces by using a Vickers hardness tester. Each test was repeated five times to verify the reproducibility of the data. The wear properties were measured on a pin-on-disk wear tester using an MMU-5G tester with a 10 kg normal force at 32 mm/s scratching speed in air. The counterbody of tribology tests was 45 steel.

3. Results and Discussion

3.1. Microstructure

Figure 2a,b show the microstructures of the Al-Bi and Al-Bi-1Sm-2Ti alloys. Al-Bi alloys are immiscible alloys, and when the alloy melt is undercooled into the miscibility gap, liquid phase separation occurs. As a result, alloy melt can separate into two melts spontaneously: the major Al-rich melt and the minor Bi-rich droplet. The liquid phase separation causes the Al-Bi immiscible alloys to have a segregated microstructure. Figure 2a shows distinct evidence for liquid phase separation with microsegregation, which is characterized by the non-dispersion of Bi-rich droplets along the direction of gravity. The Bi-rich droplets rapidly migrated along the direction of gravity due to the effect of Marangoni convection, Stokes, interface tension, and melt flow. For the Al-Bi-1Sm-2Ti alloy, as shown in Figure 2b, the Bi-rich droplets were homogeneously distributed throughout the Al matrix. The addition of elements prevents the sedimentation of the Bi-rich droplets. The size of the Bi-rich droplets decreased, and the number of Bi-rich droplets increased during the solidification processes.

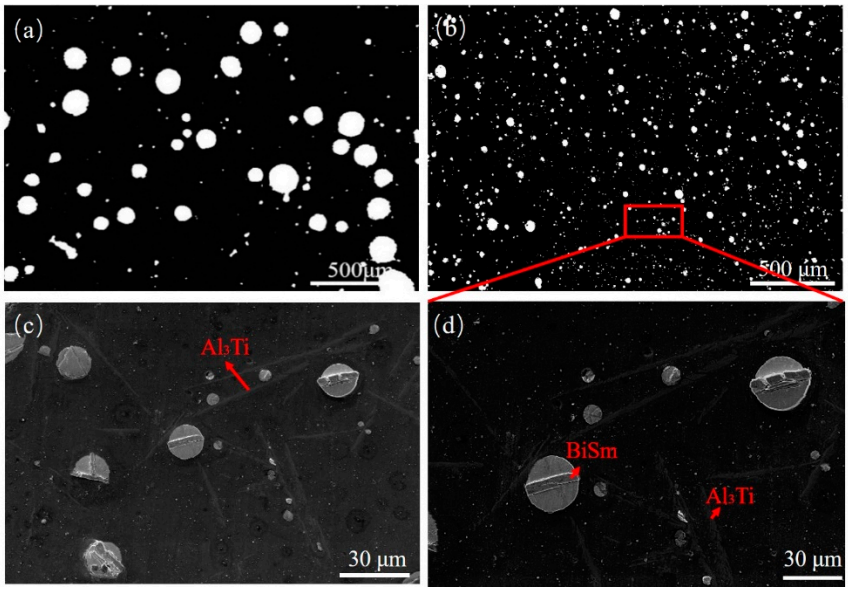


Figure 2. SEM images of the Al-Bi and Al-Bi-1Sm-2Ti alloys. (**a**) Al-Bi alloy, (**b**) Al-Bi-1Sm-2Ti alloy, (**c**,**d**) high magnification of Al-Bi-1Sm-2Ti alloy.

Figure 2c,d show the magnification of Bi-rich droplets. This indicates that most Bi-rich droplets have a rod-like phase internally. EDS analyses indicate that the rod-like phase is a BiSm intermetallic compound, which is the product of the reaction of Bi and Sm. The Al_3Ti intermetallic compounds were uniformly distributed in the matrix, as shown in Figure 2d. It can be seen that Al_3Ti intermetallic compounds were physical barriers to impede the sedimentation of Bi-rich droplets.

By comparing the microstructure of Al-Bi and Al-Bi-1Sm-2Ti alloy, such a morphological difference is fundamentally attributed to the intermetallic compounds. The intermetallic compounds were the common interfacial reaction product of Al/Ti or Sm during the high-temperature fabrication procedures. The BiSm intermetallic compounds are located inside the Bi-rich droplets due to the best wettability with the Bi-rich droplets. The refined microstructure is attributed to the in situ BiSm compounds, which act as heterogeneous nucleation sites to accelerate the nucleation of the Bi phase. The decreased size of the Bi-rich droplets led to a greater impediment to velocity, and the microsegregation of the Bi-rich droplets was restrained sharply. The Bi-rich droplets also can impede the sedimentation by Al_3Ti intermetallic compounds. Meanwhile, the uniform distribution of intermetallic compounds would reinforce the strength of the matrix. The addition of elements gave rise to the property enhancement of properties.

The XRD pattern of Al-Bi-1Sm-2Ti alloy is shown in Figure 3. The XRD pattern of Al-Bi-1Sm-2Ti alloy consisted of Al and Bi as the major phases. The patterns of Al_3Ti intermetallic compounds were detected in the alloy. The BiSm intermetallic compounds may be covered by the broad diffraction peaks of Bi phase. However, EDX analyses indicate that the BiSm intermetallic compound is located in the Bi-rich droplets, which is the product of the reaction of Bi and Sm, as shown in Figure 3b–d.

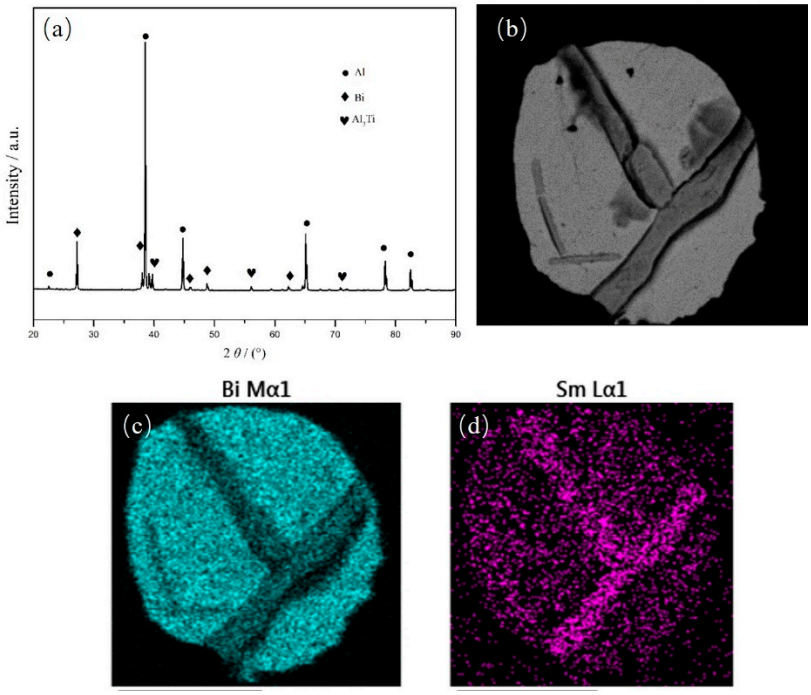


Figure 3. (**a**) XRD pattern of Al-Bi-1Sm-2Ti alloy (**b**–**d**) EDX analyses of BiSm phase.

3.2. Properties

Hardness measurements were carried out for the harness of Al-Bi alloys with different elements in Figure 4. The enhancement in the hardness value of the alloys is mainly due to the addition of Sm and Ti. It can be seen that Al-Bi alloys with Sm or Ti elements have higher hardness compared to the Al-Bi alloys, and the hardness is increased by the intermetallic compound. The hardness of Al-Bi-Sm is higher than that of Al-Bi alloy due to the in situ BiSm intermetallic compound. The hardness of Al-Bi-2Ti is higher than that of Al-Bi alloy due to the in situ Al_3Ti intermetallic compound. It is clear that the enhancement in hardness could be due to the formation of in situ and uniform distribution of intermetallic compounds in the matrix. As shown in Figure 4, Al-Bi-1Sm-2Ti alloy has the highest hardness value. The results show a significant increase in hardness values of Al-Bi-1Sm-2Ti alloy by 80.1% than that of Al-Bi alloys. This may be attributed to the better distribution of BiSm and Al_3Ti the intermetallic compounds, which provided an essential frame for plastic deformation.

To further improve the self-lubricating properties of Al-Bi alloys, the coefficient of friction and wear rate were investigated. The wear tests were conducted using a wear tester with a normal force of 10 kg and a scratching speed of 32 mm/s in air.

The variations in the coefficient of friction of Al-Bi alloys with different elements are shown in Figure 5. Continuous increase coefficient of friction is observed up to the sliding distance of 100 m, 200 m, and 300 m for Al-Bi alloys with different elements. respectively. It can be that the Al-Bi alloys with different elements' coefficient of friction are considerably less as compared to the Al-Bi alloys. This improved tribological behavior is attributed to the distribution of the Bi phase and the hardness of the matrix. The BiSm and Al_3Ti intermetallic compounds could improve the hardness of the matrix in Al-Bi alloys with

different elements. The coefficient of friction of the Al-Bi-1Sm-2Ti alloy was as low as 0.22, 37.1% lower than that of the Al-Bi alloys. The lowest friction coefficient was obtained in Al-Bi-1Sm-2Ti alloy, which was more beneficial to form a uniform Bi film in the friction contact area because the melting point of Bi was lower than that of the Al matrix.

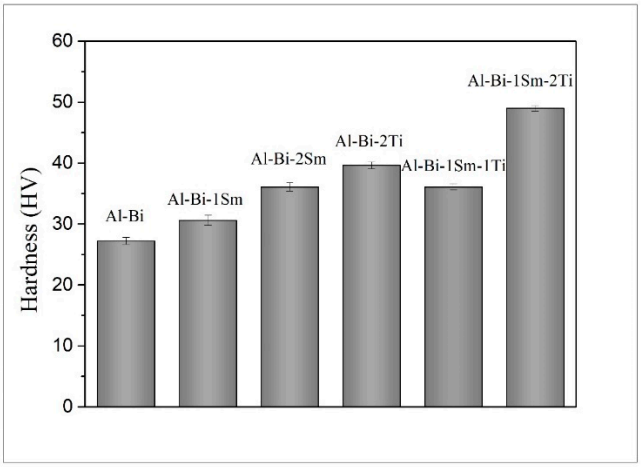


Figure 4. Hardness of Al-Bi alloys with different elements.

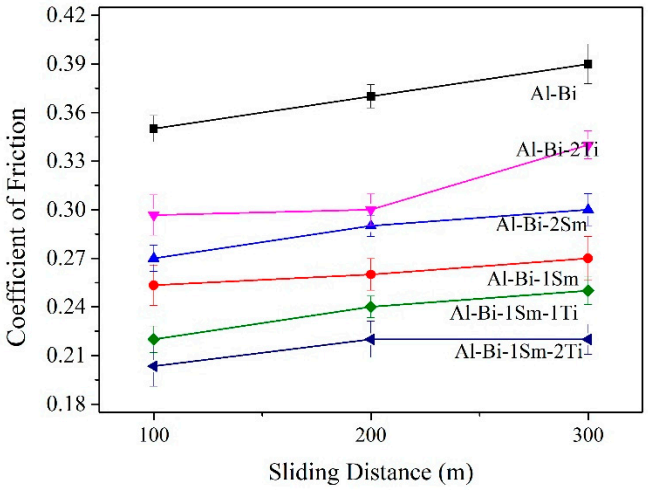


Figure 5. Variation in the coefficient of friction of Al-Bi alloys with different elements.

The equation of wear rate is as follows:

$$\text{wear rate} = \frac{\text{mass loss}}{\text{sliding distance}}$$

Figure 6 shows the variation in the wear rates of Al-Bi alloys with different elements. The wear rate decreased with the addition of elements, possibly because of the substantially increased hardness of the matrix. The wear rate of the Al-Bi-1Sm-2Ti alloy was as low as 2.0, 60.8% lower than that of the Al-Bi alloys. The main reason was that BiSm and Al_3Ti intermetallic compounds existed in the alloys, resulting in the strengthening of the matrix during friction.

The wear properties of alloys are strongly dependent on the characteristics of the microstructure formed in the solidification process. The addition of elements can improve the wear resistance by reducing the friction coefficient and wear rates of Al-Bi alloys. This is because Bi is an ideal solid lubricant, and the well-dispersed Bi-rich droplets can form an unbroken and continuous lubricating film to decrease the friction coefficient. Furthermore, the unbroken and continuous lubricating film protects the matrix from mass loss. In terms

of strength, large amounts of intermetallic compounds are dispersed within the Al matrix, resulting in dispersion strengthening. The microstructure of Al-Bi-1Sm-2Ti alloys led to substantial improvement in the friction and wear performance, as indicated by the lower friction coefficient and much lower wear loss than those of the Al-Bi alloys. Dislocation glide is inhibited by the abundant intermetallic compounds when glide dislocations encounter these intermetallic compounds.

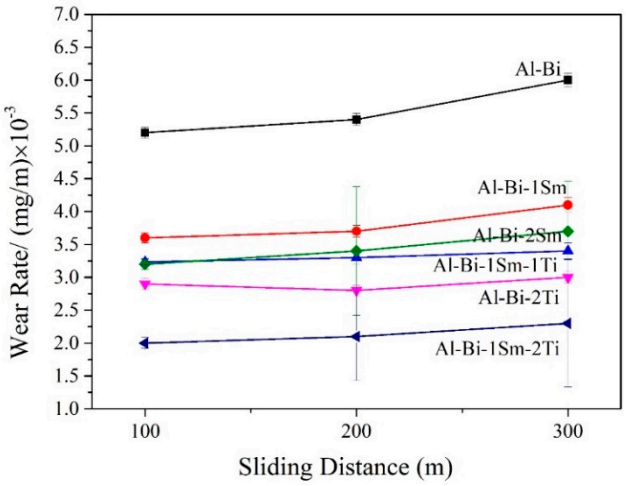


Figure 6. Variation in the wear rate of Al-Bi alloys with different elements.

The wear behavior implies different operating wear mechanisms and thus different microstructural evolution of the sliding interfaces. Figure 7 shows the worn surface morphology of Al-Bi and Al-Bi-1Sm-2Ti alloys sliding against low-carbon steel. The worn surfaces reveal substantial differences between the Al-Bi and Al-Bi-1Sm-2Ti alloys. For Al-Bi alloys, the dry sliding worn surface consisted of particle packing and grooves along the direction of wear, as shown in Figure 7a. Large-scale particle packings indicate that the wear mode is mainly abrasive wear, which is attributed to the lower microhardness. The grooves were produced by plastic deformation, which caused a notable increase in wear rate. As shown in Figure 7b, the grooves were remarkably reduced in the worn surface for the Al-Bi-1Sm-2Ti alloys, which possibly originated from the improvement in the hardness and strength of the matrix. The variation tendency of the wear surfaces was similar to that of the friction coefficient and wear rates of the Al-Bi and Al-Bi-1Sm-2Ti alloys. After the addition of elements, the wear mechanism was transformed from adhesive wear and abrasive wear to the joint action of adhesive wear.

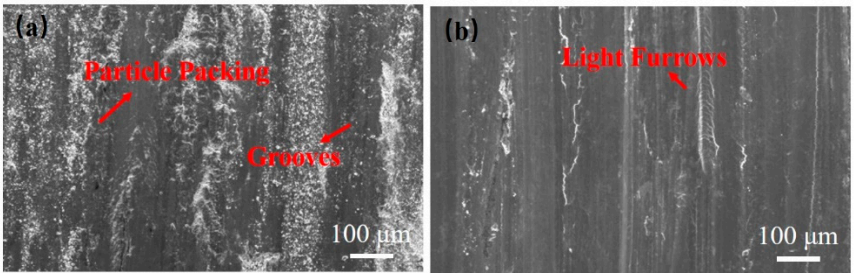


Figure 7. SEM micrographs of the worn surface of (**a**) Al-Bi alloys and (**b**) Al-Bi-1Sm-2Ti alloys.

The results indicated that the wear properties were improved with the addition of elements. On the one hand, this can be attributed to the high hardness of the intermetallic compound, leading to the formation of a highly intensified area. The friction coefficient and wear rates decreased. During the wear process, intermetallic compounds protruded gradually and suffered friction, preventing the surface from further abrasion. The inter-

metallic compounds were widely distributed on the worn surface and had excellent wear resistance, making the surface difficult to cut.

On the other hand, the well-dispersed Bi-rich droplets were extruded into the wear surface of the Al-Bi-1Sm-2Ti alloys due to the compressive stress. Then, a lubricating film including a large amount of Bi-rich droplets was formed on the surface. A low shearing stress easily formed on the sliding interface of the Bi tribo-film. The Bi-rich friction films had better wear and friction resistance, causing the Al-Bi-1Sm-2Ti alloy to have excellent tribological properties.

3.3. Solidification Microstructure

Liquid phase separation depends primarily on the composition, surface segregation, and Stokes and Marangoni motions. The Bi-rich droplets in Al-Bi immiscible alloys nucleate and grow driven by the Stokes effect due to the large difference in density. Meanwhile, the Bi-rich droplets in the same horizontal plane immigrate to the high-temperature central region driven by Marangoni motion. The Bi-rich droplets collide with each other and combine, forming a big droplet due to the Stokes convection and Marangoni convection. In order to understand the solidification process of the Al-Bi and Al-Bi-1Sm-2Ti alloys, a model is developed to calculate the position and velocity of Bi-rich droplets in the melt. The nucleation rates of Bi-rich droplets in the Al-Bi and Al-Bi-1Sm-2Ti alloys were measured by quenching. The microstructure formation of Al-Bi and Al-Bi-1Sm-2Ti alloys under different times were numerically simulated by the dispersing particle method [22].

The motion of droplets can be described on the basis of Newton's second law of motion under the various forces:

$$\frac{d(g\rho_p U_p)}{dt} = \sum \underset{F}{\rightarrow}$$

where g is the gravitational acceleration, rp is the density of droplets, Up is the instantaneous velocity of a droplet, and F denotes the various forces.

$\underset{F}{\rightarrow}$ include buoyancy force, viscosity drag force, and interfacial gradient force:

$$\sum \underset{F}{\rightarrow} = \underset{F_{buo}}{\rightarrow} + \underset{F_{maran}}{\rightarrow} + \underset{F_{drag}}{\rightarrow}$$

Buoyancy force depends on the density difference between droplets and the matrix:

$$\underset{F_{buo}}{\rightarrow} = g(\rho_m - \rho_p) \underset{e_x}{\rightarrow}$$

where $\underset{e_x}{\rightarrow}$ is a unit vector in the direction of gravity, ρ_m and ρ_p are the density of Al and Bi-rich droplets, respectively.

Drag forces are described by the following equation:

$$\underset{F_{drag}}{\rightarrow} = -2\pi R\eta_m \left(\underset{U_P}{\rightarrow} - \underset{U_m}{\rightarrow} \right) \frac{2\eta_m + 3\eta_P}{\eta_m + \eta_P}$$

where η_m and η_P are the dynamic viscosities of the matrix and Bi-rich droplets, respectively. $\underset{U_m}{\rightarrow}$ and $\underset{U_P}{\rightarrow}$ are the flow velocity of the matrix and Bi-rich droplets.

The Marangoni motion is driven by the interfacial gradient force following the equation:

$$\underset{F_{maran}}{\rightarrow} = -\frac{4\pi R^2}{(1 + \eta_P/\eta_m)(2 + \lambda_P/\lambda_m)} \frac{\partial \delta}{\partial T} \nabla T$$

where λ_m and λ_P are the thermal conductivity of the matrix and droplets, respectively. ∇T is the temperature gradient. δ is the interfacial tension. The direction of the Marangoni force is the same as the temperature gradient.

The growth rate of Bi-rich droplets can be written as:

$$\frac{dR}{dt} = \frac{x_{Bi} - x_{Bi}^{m}}{x_{Bi}^{P} - x_{Bi}^{m}} \frac{8}{\sqrt{3\pi}} D_{Bi^{1/2}} (U_P - U_m)^{1/2} R^{-1/2}$$

where is the diffusion coefficient of Bi in the Al matrix. x_{Bi} is the concentration of Bi in the matrix surrounding the growing Bi-rich droplets. x_{Bi}^{m} and x_{Bi}^{P} are the mole fractions of component Bi in the matrix and droplets, respectively.

The concentration Bi can be written as:

$$R_{Bi} = \sum \frac{4}{3} \pi \rho_P \left[\left(R + \frac{dR}{dt} \right)^3 - R^3 \right]$$

The size and position of each Bi-rich droplet are memorized. The number of droplets up to 2×10^5, the data is used to compare with the experiments by the same conditions. Figure 8 shows the solidification microstructure of Al-Bi and Al-Bi-1Sm-2Ti alloys. The Bi-rich droplets are homogeneous distribution at 0 s both Al-Bi and Al-Bi-1Sm-2Ti alloys. At 0.5 s, the number of droplets in Al-Bi-1Sm-2Ti alloys was more than that in Al-Bi alloys due to the in situ intermetallic compound. At 1 s, the size of Bi-rich droplets in Al-Bi alloys was larger than that in Al-Bi-1Sm-2Ti alloys, which indicates that the velocity of coarsening in Al-Bi alloys was fast. The lower velocity of coarsening in Al-Bi-1Sm-2Ti alloys leads to intermetallic compounds. The BiSm intermetallic compounds were effective inoculants for the nucleation of the Bi phase. Therefore, the addition of Sm accelerates the nucleation rate of the Bi phase by the heterogeneous nucleation sites due to its wettability.

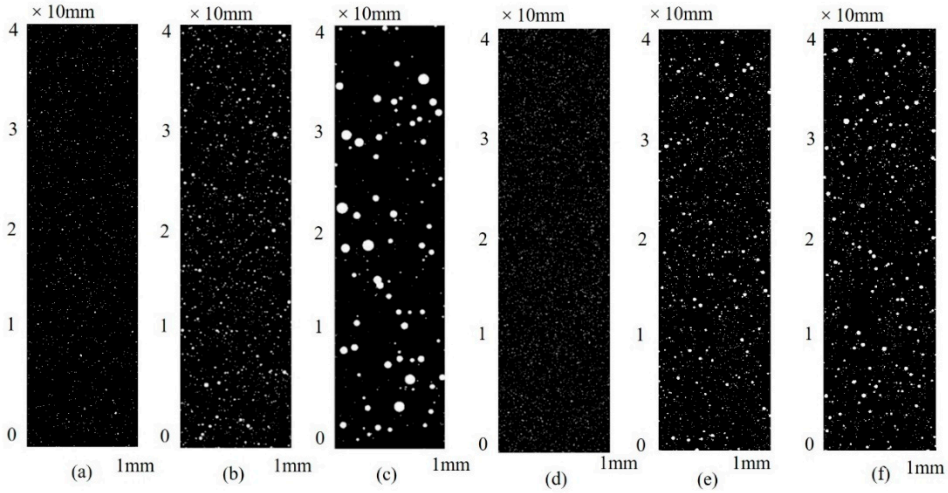


Figure 8. Spatial microstructure evolutions of Bi-rich droplets. Al-Bi alloy (**a**) 0 s; (**b**) 0.5 s; (**c**) 1 s; Al-Bi-1Sm-2Ti alloy (**d**) 0 s; (**e**) 0.5 s; (**f**) 1 s.

The nucleation of the Bi with the intermetallic compounds can be described by the classical heterogeneous nucleation theory. The heterogeneous nucleation rate of the precipitated phase can be calculated as follows [20]:

$$I_{heter} = N_V N_0 O \Gamma Z exp\left[-f(\theta) \frac{\Delta G_C}{k_B T} \right]$$
$$f(\theta) = \frac{2 - 3\cos\theta + \cos\theta^3}{4}$$

where I_{heter} is the heterogeneous nucleation rate; N_V is the concentration of the catalyzing impurities; N_0 is the number density of atoms in the liquid; ΔG_C is the Gibbs free energy on homogeneous nucleation; $\Gamma = 6D/\lambda^2$ is the attachment rate of atoms to droplets; with D being the diffusion coefficient and λ the average diffusional jump distance of the atoms; Z is the Zeldovich factor; $O = 4n_c^{2/3}$ which reflects the surface area of the nuclei; with n_c

being the number of atoms in a droplet of critical radius; θ is the contact angle between the intermetallic compound and the Bi-rich droplet located inside the Al matrix; K is the Boltzmann constant; and T is the temperature. θ is determined by the interfacial energy, and describes the energy barrier to nucleation owing to the wettability. The Bi phase nucleates on the BiSm intermetallic compounds due to the excellent wettability. Therefore, the BiSm intermetallic compound accelerates the nucleation rate of the Bi phase by the heterogeneous nucleation sites. The velocity of Bi droplets decreases also owing to the rapid nucleation, which is beneficial for suppressing the coalescence by Al_3Ti intermetallic compounds. The Al_3Ti intermetallic compounds are physical barriers to the sedimentation of Bi-rich droplets. The homogeneous microstructure of Al-Bi-1Sm-2Ti alloys led to substantial improvement in the friction and wear performance, as indicated by the lower friction coefficient and much lower wear loss than those of the Al-Bi alloys.

4. Conclusions

The high self-lubricating performance of Al-20Bi-1Sm-2Ti alloys was fabricated. The results of both the experiment and model calculation indicated the solidification process of Al-Bi and Al-Bi-1Sm-2Ti alloys. The distribution of Bi-rich droplets remarkably changes from segregated to well-dispersed based on the intermetallic compounds. The experimental results reveal that the BiSm and Al_3Ti intermetallic compounds are effective for retarding the sedimentation of the Bi-rich droplets. The BiSm intermetallic compounds act as heterogeneous nucleation sites due to their wettability. The Al-Bi-1Sm-2Ti alloys possess the most excellent self-lubricating wear properties with well-dispersed soft Bi-rich droplets and a harder matrix. The numerical model indicates the coarsening mode and the microstructural evolution under liquid phase separation in the Al-Bi-1Sm-2Ti alloys.

Author Contributions: T.M. designed the experiments; T.M. and Z.N. performed the experiments; L.Z. analyzed the data; E.W. contributed reagents/materials/analysis tools; T.M. wrote the paper; S.L. and E.W. modified the article; Z.N. financial support. All authors have read and agreed to the published version of the manuscript.

Funding: This research was funded by Northeastern University EPM Open Projects NEU-EPM-019 and Liaoning Provincial Department of Education projects LJKMZ20220570.

Data Availability Statement: Not applicable.

Acknowledgments: This work was supported by Northeastern University EPM Open Projects NEU-EPM-019 and the Liaoning Provincial Department of Education projects LJKMZ20220570.

Conflicts of Interest: The authors declare no conflict of interest.

References

1. Zhao, D.G.; Liu, R.X.; Wu, D.; Bo, L.; Wang, L. Liquid-liquid phase separation and solidification behavior of Al-Bi-Sb immiscible alloys. *Results Phys.* **2017**, *7*, 3216–3221. [CrossRef]
2. Zhou, B.; Lin, W.; Guo, Y.; Zheng, T.; Zhong, Y.; Zhang, L.; Zhang, Q. Tailoring homogeneous immiscible alloy via magneto-Archimedes levitation. *Scr. Mater.* **2023**, *226*, 115268. [CrossRef]
3. Sun, X.; He, J.; Chen, B.; Zhang, L.; Jiang, H.; Zhao, J.; Hao, H. Microstructure formation and electrical resistivity behavior of rapidly solidified Cu-Fe-Zr immiscible alloys. *J. Mater. Sci. Technol.* **2020**, *44*, 201–208. [CrossRef]
4. Verma, N.; Pant, N.; Beach, J.A.; Ivanisenko, J.; Ashkenazy, Y.; Dillon, S.; Bellon, P.; Averback, R.S. Effects of ternary alloy additions on the microstructure of highly immiscible Cu alloys subjected to severe plastic deformation: An evaluation of the effective temperature model. *Acta Mater.* **2019**, *170*, 218–230. [CrossRef]
5. Jiang, H.; Li, S.; Zhang, L.; He, J.; Zhao, J. Effect of microgravity on the solidification of aluminum-bismuth-tin immiscible alloys. *NPJ Microgravity* **2019**, *5*, 26. [CrossRef]
6. Xie, M.; Zhou, S.; Zhao, S.; Jin, J.; Chen, D.; Zhang, L.C. In-situ Fe_2P reinforced bulk Cu-Fe immiscible alloy with nanotwinned Cu produced by selective laser melting. *J. Alloys Compd.* **2020**, *838*, 155592. [CrossRef]
7. Deng, C.; Jiang, H.; Zhao, J.; Zhang, L.; He, J. Thermodynamics and solidification kinetics of Ag-Ni-Co immiscible alloys. *J. Mater. Sci.* **2021**, *56*, 3455–3471. [CrossRef]
8. Peng, Y.L.; Wang, Q.; Wang, N. A comparative study on the migration of minor phase globule in different-sized droplets of Fe-58wt%Sn immiscible alloy. *Scr. Mater.* **2019**, *168*, 38–41. [CrossRef]

9. Zhou, S.; Xie, M.; Wu, C.; Yi, Y.; Chen, D.; Zhang, L.C. Selective laser melting of bulk immiscible alloy with enhanced strength: Heterogeneous microstructure and deformation mechanisms. *J. Mater. Sci. Technol.* **2022**, *104*, 81–87. [CrossRef]
10. Costa, T.A.; Freitas, E.S.; Dias, M.; Brito, C.; Cheung, N.; Garcia, A. Monotectic Al/Bi-Sn alloys directionally solidified: Effects of Bi content, growth rate and cooling rate on the microstructural evolution and hardness. *J. Alloys Compd.* **2015**, *653*, 243–254. [CrossRef]
11. Wu, Y.; Su, J.; Zhang, L.; Du, M. Observations and simulations for phase separation process of immiscible $Fe_{50}Sn_{50}$ alloy droplets placed on a chilling surface. *J. Alloys Compd.* **2023**, *947*, 169565. [CrossRef]
12. Zhao, B.; Zhang, L.; Wu, M.; Li, S.; Zhai, Q.; Gao, Y. Heterogeneous nucleation of embedded droplets in the Zn-15Bi immiscible alloy studied by nanocalorimetry. *Thermochim. Acta* **2023**, *720*, 179420. [CrossRef]
13. Li, Y.; Xia, W.; Wang, X.; Ju, Y.; Liu, T.; Zhao, D.; Zuo, M. Effects of cooling rate on the microstructure control and liquid–liquid phase separation behavior of Cu-Fe-P immiscible alloys. *Mater. Today Commun.* **2022**, *33*, 104300. [CrossRef]
14. Cao, S.; Lu, W.; Hu, Q.; Yu, P.; Ge, X.; Lai, P.; Li, J. Atomic tuning effect of TiB 2 particles on the liquid phase separation behavior of an Al-Bi immiscible alloy. *Scr. Mater.* **2022**, *209*, 114365. [CrossRef]
15. Chen, L.Y.; Xu, J.Q.; Choi, H.; Konishi, H.; Jin, S.; Li, X.C. Rapid control of phase growth by nanoparticles. *Nat. Commun.* **2014**, *5*, 3879. [CrossRef]
16. Cao, C.; Chen, L.; Xu, J.; Zhao, J.; Pozuelo, M.; Li, X. Phase control in immiscible Zn-Bi alloy by tungsten nanoparticles. *Mater. Lett.* **2016**, *174*, 213–216. [CrossRef]
17. Sun, Q.; Jiang, H.; Zhao, J.; He, J. Microstructure evolution during the liquid-liquid phase transformation of Al-Bi alloys under the effect of TiC particles. *Acta Mater.* **2017**, *129*, 321–330. [CrossRef]
18. Peng, Y.L.; Han, S.X.; Tian, L.L.; Wang, N. In situ investigation of minor-phase globule collision and the structure in a droplet-shaped immiscible alloy. *Mater. Lett.* **2019**, *254*, 222–225. [CrossRef]
19. Wei, C.; Wang, J.; He, Y.; Li, J.; Beaugnon, E. Influence of high magnetic field on the liquid-liquid phase separation behavior of an undercooled Cu-Co immiscible alloy. *J. Alloys Compd.* **2020**, *842*, 155502. [CrossRef]
20. Ratke, L. Coarsening of liquid Al-Pb dispersions under reduced gravity conditions. *Mater. Sci. Eng.* **1995**, *A203*, 399. [CrossRef]
21. Kaban, I.G.; Hoyer, W. Characteristics of liquid-liquid immiscibility in Al-Bi-Cu, Al-Bi-Si, and Al-Bi-Sn monotectic alloys: Differential scanning calorimetry, interfacial tension, and density difference measurements. *Phys. Rev.* **2008**, *77B*, 125426. [CrossRef]
22. Zhang, L.; Man, T.; Huang, M.; Gao, J.; Zuo, X.; Wang, E. Numerical Simulation of Droplets Behavior of Cu-Pb Immiscible Alloys Solidifying under Magnetic Field. *Materials* **2017**, *10*, 1005. [CrossRef] [PubMed]

Disclaimer/Publisher's Note: The statements, opinions and data contained in all publications are solely those of the individual author(s) and contributor(s) and not of MDPI and/or the editor(s). MDPI and/or the editor(s) disclaim responsibility for any injury to people or property resulting from any ideas, methods, instructions or products referred to in the content.